# Fault detection for scraper chain using an observer-based tension distribution estimation algorithm

## Xing Zhang, Wei Li*, Zhencai Zhu and Fan Jiang

School of Mechatronic Engineering, China University of Mining and Technology, Xuzhou 221116, China and
Jiangsu Key Laboratory of Mine Mechanical and Electrical Equipment, China University of Mining and Technology, Xuzhou 221116, China

**Here we describe a fault detection scheme for a scraper chain based on a new tension distribution estimation algorithm (TDEA). A multi-body dynamic model of the ring chain transmission system (RCTS) has been developed to simulate the actual production environment of the scraper conveyer, and the fixed-point strain measurement experiment was conducted to validate the system performance of the dynamic model. Because of the difficulties with direct measurement and restrictions of high-cost tension sensors, TDEA was achieved using a mathematical model-based linear state observer for practical applications to monitor tension variation of the scraper chain. Moreover, the desired observer makes it feasible to obtain all the contact forces between ring chains based on the measurable state variables. For research purpose, the proposed fault detection scheme is applicable in detecting chain faults by monitoring the working state of the scraper chain. Theoretical analysis and simulation results show that the developed method is efficient to detect the occurrence of chain failure.**

**Keywords:** Dimension-minimized algorithm, multi-body dynamics, tension monitoring, tension distribution estimation.

THE scraper conveyor has applications in many fields such as metallurgy, aerospace, building materials, mining, etc. As described in Figure 1, a coal scraper conveyor is an important mechanical transportation equipment with a chain-type traction underground fully mechanized mining face. Its reliability and efficiency can be directly related to the production performance of the ring chain transmission system (RCTS). Mainly composed of the driving system, sprockets, scrapers, ring chains and middle troughs, the RCTS has attracted much attention regarding the complex interactions between different components. Researchers have conducted relatively thorough studies on the multi-body dynamics of different systems[1–3]. These studies provided a foundation for the research on the RCTS. Wauge[4] presented a simplified re-

presentation of the RCTS and explored the dynamic behaviour of both drive types and their effect on chain tension. Nie et al.[5] divided the RCTS into multiple space-fixed finite control volumes, and derived the governing equations of objects in these control elements using the Newton-Euler approach. He et al.[6] studied the contact characteristics of two chains by finite element analysis. Jiang et al.[7] performed multi-body rigid and rigid-flexible coupling simulations of the chain assembly to determine the dynamic properties of the RCTS. To the best of our knowledge, there is no published work that explicitly studied the dynamic behaviour of double-chain RCTS.

Generally, the tension variation of the scraper chain can effectively reflect the working state of the RCTS. Several researchers have focused on the study of tension characteristics over the past decade. Myszkowski et al.[8] estimated the essential operating parameters using a mobile measuring system. Wang et al.[9] developed a set of tension testing systems of the scraper conveyor based on micro-strain detection. In addition, with increasing concerns about the estimation method, the theory of state observer has been widely applied in various fields[10–12]. Considering the present research situation, there is restriction on direct multi-point measurements of chain tension because of the high-cost testing equipment and difficulty in installation. To date, there are few studies on tension estimation of the RCTS, and tension monitoring of multi-point scraper chains has not been considered.

Due to poor running condition, problems with the operation of the scraper chain occur frequently, hindering coal safety and high efficiency production during chain usage and maintenance. This will eventually lead damage of the sprockets, scrapers, ring chains and middle troughs, as well as over current and overload of the drive motors. Accordingly, fault detection of the scraper conveyor is important and of great significance. Presently, many methods have been employed for performing fault detection. Sun et al.[13] proposed a new fault diagnosis analysis strategy for a coal scraper conveyor accident. Zhang et al.[14] proposed the fuzzy neural network fault diagnosis scheme and designed an on-line fault monitoring system for the scraper conveyor. Gong et al.[15] introduced a model that integrated breakdown extraction, failure

*For correspondence. (e-mail: liwei_cmee@163.com)

diagnosis and fault analysis in the large-scale scraper chain conveyor breakdown. Xue et al.[16] combined fault tree and Bayesian network through failure rate for completing the fault diagnosis of the scraper conveyor. In addition, the fault diagnosis and maintenance method based on linear observer has attracted intensive attention. Sedighi et al.[17] proposed a fault detection scheme to detect intermittent faults based on the designed observer. Emami et al.[18] presented a functional observer-based fault detection technique for dynamical systems. Currently, most of the research stops proceeding at the level of theoretical algorithms and heuristics obtained via experience and thus is not suitable for engineering applications. Moreover, few studies on observer-based chain faults detection of RCTS have been performed.

In this article, we describe a virtual prototype model of the double-chain RCTS based on the multi-body dynamics theory using ADAMS software, which serves as a dynamic model to study the incidence relations between the dynamic characteristics and running states of the actual RCTS under normal working conditions. The efficiency of the dynamic model is verified by experimental study. Sequentially, a combination of mass-spring-damping modules and the MATLAB package is implemented to establish the mathematical model of RCTS. This model has been applied to design the linear state observer. In this study, to monitor the tension variation of RCTS, we introduce an observer-based tension distribution estimation algorithm (TDEA) that allows for estimation of the tension variation of all scraper chains based on the measurable chain forces. By comparing the estimated tension value and actual tension value obtained from the virtual prototype model, the effectiveness of the TDEA is validated. The achieved fault detection scheme for the scraper chain based on TDEA is utilized to determine the types of chain faults; these are mainly divided into two types – chain breakage and chain jam. According to the

simulation results, the fault detection scheme for the scraper chain shows excellent performance to detect the occurrence of chain failure.

## Dynamic modelling of RCTS

In this study, a virtual prototyping model is built and is specifically adapted to evaluate the interactions between the main components of an actual RCTS. Moreover, the mathematical model is established, based on which the linear state observer can be constructed.

### Multi-body dynamic model

To model contacting bodies of the RCTS, the contact pairs are built based on the polygonal contact model (PCM)[19]. The PCM functions as a representative contact algorithm to solve contact problems and can consider complex contact surfaces with satisfactory results using the hypothesis that elastic components in RTCS can be treated as rigid bodies.

In this study, the dimension of ring chains is $\varnothing\,48 \times 152$ (mm). In fact, a great number of contacting bodies are included because of the complex structure of the scraper conveyor, such as the sprockets, ring chains, scrapers, transitional troughs and middle troughs. Referring to the PCM theory, contact pairs occur between two relatively moving rigid bodies and is effectively used for dynamic modelling of the actual RCTS.

Constructed using ADAMS software, the dynamic model of RCTS consists of three prominent systems: a double-chain system, a transmission trough system and a double-drive sprocket system (Figure 2 a). The double-chain system is composed of the left single-chain subsystem and the right single-chain subsystem, and both subsystems can be divided into plat chains, scrapers and vertical chains. The transmission trough functions as an
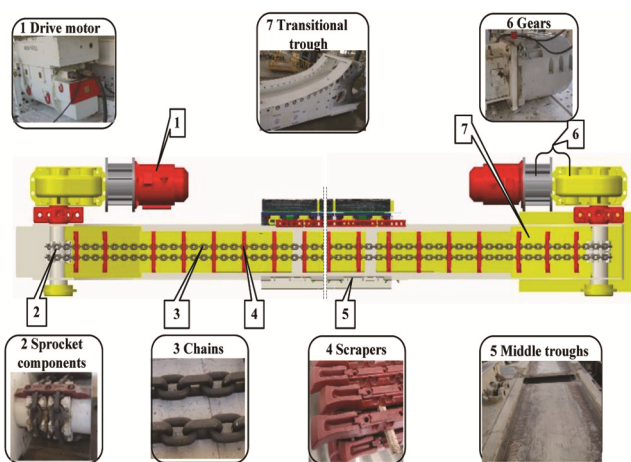


**Figure 1.** Schematic diagram of the coal scraper conveyor.
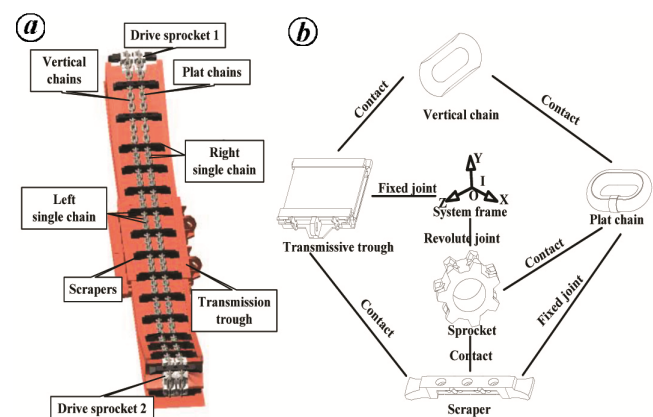


**Figure 2 a, b.** Multi-body dynamic modelling of the ring chain transmission system.

independent body. To describe the interactions between two rigid bodies definitely, the kinematic restriction includes two main aspects: kinematic constraints and contact relations (Figure 2 b). As the actual double-drive transmission system is driven by an electromotor, we apply rotation motion on the revolute joints, which are built between the drive sprocket and the system frame. To ensure compliance with the working conditions of the actual RCTS, we take the rotation angular velocities of the two sprockets as the inputs. After a smooth and steady start-up process （0–1 s), the drive sprockets rotate at a steady speed of 2.56 rad/s (1–4.1 s). Based on multibody dynamics simulation, the driving torques of sprockets 1 and 2 are represented as $T_h$ and $T_t$ respectively (Figure 3). For further analysis, $T_h$ and $T_t$ serve as the inputs of the mathematical model.

*Establishment of the mathematical model*

Under the effects of uniform load, the left single-chain subsystem and the right single-chain subsystem operate as a closed transmission system formed by linking the ring chains together, and are similar in kinematic and dynamic behaviours. In this study, contact pairs are mainly considered between the sprocket and plat chain, and between the vertical chain and plat chain. To explore the instantaneous impact forces of the contact pairs, we discretize the left single-chain subsystem into a system of Kelvin models according to the viscoelastic properties of the ring chains. Moreover, the one-dimensional longitudinal discrete system is obtained through the finite element method to study the longitudinal dynamic characteristics of the RCTS (Figure 4).

In Figure 4, the sprocket rotates in the counter-clockwise direction, and $n$ discrete elements are modelled as Kelvin modules and assumed to be elastically connected to each other. Dominated by elasticity and damping, the viscoelastic model allows force transfer between contiguous elements. To study dynamic behaviour of the system, mathematical equations are constructed

$$m_1 x_1'' + (c_1 + c_n + f_1)x_1' - c_1 x_2' - c_n x_n'$$

$$+ (k_1 + k_n)x_1 - k_1 x_2 - k_n x_n = T_t/R_t, \tag{1}$$

$$m_{n/2+1} x_{n/2+1}'' + (c_{n/2} + c_{n/2+1} + f_{n/2+1})x_{n/2+1}'$$

$$- c_{n/2} x_{n/2}' - c_{n/2+1} x_{n/2+2}' + (k_{n/2} + k_{n/2+1})x_{n/2+1}$$

$$- k_{n/2} x_{n/2} - k_{n/2+1} x_{n/2+2} = T_h/R_h, \tag{2}$$

$$m_j x_j'' + (c_{j-1} + c_j + f_j)x_j' - c_{j-1}x_{j-1}' - c_j x_{j+1}'$$

$$+ (k_{j-1} + k_j)x_j - k_{j-1}x_{j-1} - k_j x_{j+1} = 0, \tag{3}$$

$$m_n x_n'' + (c_{n-1} + c_n + f_n)x_n' - c_{n-1}x_{n-1}' - c_n x_1'$$

$$+ (k_{n-1} + k_n)x_n - k_{n-1}x_{n-1} - k_n x_1 = 0, \tag{4}$$

where $x_j$, $x_j'$, $x_j''$, $m_j$, $k_j$, $c_j$ and $f_j$ represent the displacement, velocity, acceleration, equivalent mass, stiffness coefficient, damping coefficient and resistance coefficient of discrete element $j$ respectively. Here, $T_h$ and $T_t$ are the driving torques of the sprockets at the head and tail of the discrete system respectively. $R_h$ and $R_t$ are the driving radii of the sprockets. For $j = 1$ and $j = n/2 + 1$, mathematical equations of the elements are described as given in eqs (1) and (2) respectively. For $2 \leq j \leq n/2$ and $n/2 + 1 \leq j \leq n - 1$, the dynamic behaviour of element $j$ is described as given eq. (3). Moreover, eq. (4) is applied for element $n$. Based on the above, we build the differential equations of the time-invariant linear system as
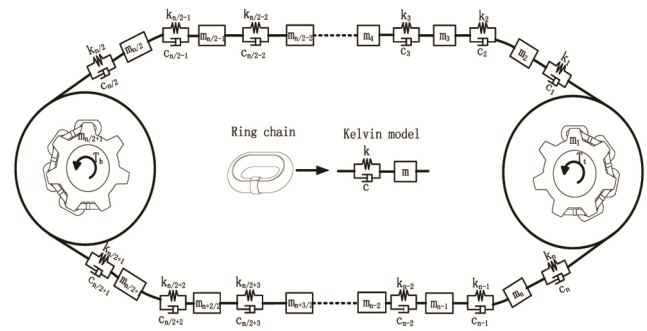
$$Z' = AZ + BU, \tag{5}$$

$$Y = HZ. \tag{6}$$

where $A$, $B$, $Y$ and $H$ are the constant system matrix, control matrix, output matrix and transformation matrix
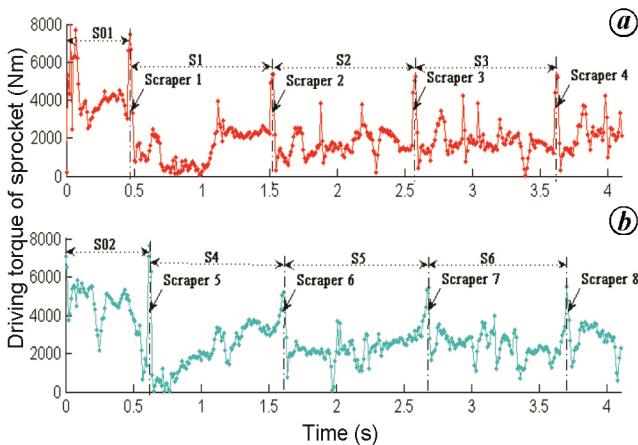


**Figure 3.** Driving torque of (*a*) sprocket 1 ($T_h$); (*b*) sprocket 2 ($T_t$).



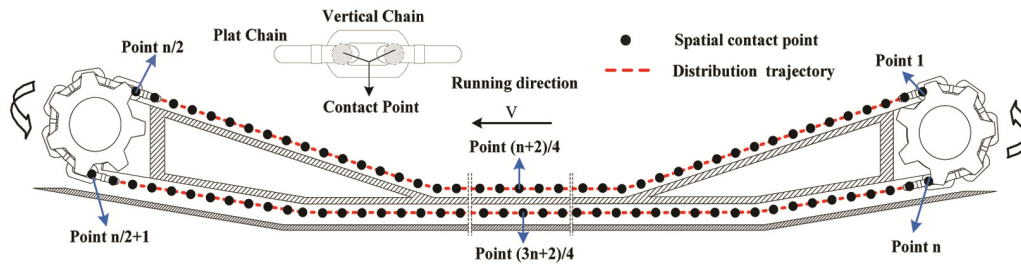**Figure 4.** Longitudinal discrete system of the left single-chain subsystem.

**Figure 5.** Spatial distribution of the contact points.

respectively. $Y$ is defined as the output matrix, $Z$ is the state matrix and $U$ is the input matrix. Here, numerical solutions of the state-space model can be derived using the fourth-order Runge-Kutta formula[20].

### Tension distribution estimation

#### Spatial distribution of contact points

In this study, surface-to-surface contact pairs are defined between two contacting bodies to analyse the transient dynamic characteristics of the actual RCTS. As the surfaces of the contact pairs are irregular and changing constantly, the contacting surfaces are represented as simplified contact points, and positions of the contact pairs can be transformed into a closed spatial tension distribution trajectory (Figure 5). The simplified spatial contact points move relative to the system frame, with the positive direction chosen as the direction of the arrow. For ease of study, each contact point $i(1 \le i \le n)$ is specifically numbered, based on which we define the distribution trajectory with a certain shape. Accordingly, tension monitoring of RCTS can be smoothly transformed into the study of the longitudinal contact forces of contact pairs at certain spatial points.

#### Observer-based tension distribution estimation algorithm

For the actual RCTS, to obtain all contact force values of contact pairs, many tension sensors are required. This results in contradiction between practical engineering requirements and measurement restrictions. Aiming to solve the above contradiction and monitor tension variation of the RCTS, the observer-based TDEA is designed to estimate unmeasurable contact forces of the actual RCTS through the available states. The proposed TDEA includes two major parts, i.e. construction of the state observer, and design of a novel dimension-minimized algorithm.

As designed, the left single-chain subsystem is modelled as $n(n = 146)$ discrete elements by Kelvin model in series connections. Based on the mathematical model, we get the state observer as

$$\bar{Z}' = (A - GH)\bar{Z} + BU + GY, \tag{7}$$

$$\bar{Y} = \tilde{H}\bar{Z}, \tag{8}$$

where $\bar{Z}$ serves as the $2n \times 1$ reconstructed state matrix

$$\bar{Z} = [\bar{x}_1; \ \bar{x}_2; \cdots \bar{x}_{n/2+1}; \cdots \bar{x}_{n-1};$$

$$\bar{x}_n; \bar{x}'_1; \bar{x}'_2; \cdots \bar{x}'_{n/2+1}; \bar{x}'_{n-1}; \bar{x}'_n]_{2n \times 1}.$$

$U$ and $Y$ are the input matrices. $\tilde{H}$ is the $2n$-order identity matrix. $H$ is the $q \times 2n$ sensor calibration matrix $G$ is the $q \times n$ feedback gain matrix. $q$ denotes the number of available states corresponding to the number of tension sensors. $Y$ serves as the state feedback of the state observer and works as the available states, which can be derived from direct measurement by $q$ tension sensors. $\bar{Y}$ is the reconstructed output matrix which serves as the estimation results.

With high relevance in applications, we can finally estimate the change rules of displacement, velocity, acceleration and contact force of all discrete elements (Figure 4) at any time $t$. Further, we can obtain the tension variation of the actual RCTS by replacing the unmeasurable contact forces with observed results. The designed observer has a heavy computational load due to high dimensionality of the state matrix. Based on our previous work[21], we develop a new dimension-minimized algorithm to reduce the dimension of the observer, where the $M_0$-order observer is reconstructed by $T_0$ elements. The left single-chain subsystem can be grouped into two parts to depict, the upper and lower chain subsystems, represented by contact points $I_1(1 \le I_1 \le n/2)$ and $I_2(n/2 + 1 \le I_2 \le n)$ respectively. Based on the reconstructed observer, we can finally achieve the research goal of estimating the contact forces of all the $n$ spatial contact points of the actual RCTS.

### Fault detection of the scraper chain

The scraper conveyor operates in harsh environments and is affected by frequent loading, excessive bending and improper operation. Due to unexpected variations in the external surroundings and other uncertain factors, different types of chain faults usually act on the system during normal operations. The fundamental idea of our approach

is to generate an alarm when a fault occurs and avoid the eventual damage. This method not only estimates tension variation, but also detects chain failure of the RCTS.

*Experimental study*

The fixed-point experimental strain measurement of the scraper chain was conducted to obtain the working conditions and evaluate the dynamic performance of the RCTS. The main purpose of the experimental study includes verification of the multibody dynamic model and evaluation of chain faults. The specifications of the experimental scraper conveyor correspond to SGB1200/3600 (Lianyungang Tianming Equipment Co. Ltd, China) and running speed of the scraper and chain is 1.0 m/s without load. As shown in Figure 6, the experimental system mainly consists of strain gauges, a wireless data acquisition device, wireless transmitter, wireless receiver and an on-site PC.

With obvious advantages, strain gauges (SAK120) are used for fixed-point experimental strain measurements by detecting the strain responses of the scraper chain along the running direction during the experiment, with the size of the sensor elements being restricted by the limited installation space. The locations of the strain measuring points are shown in Figure 6, and two strain gauges are installed on the upper surface of the tested vertical chain by epoxy adhesive at sensor points 1 and 2. Mounted on the upper surface of the scraper by four magnetic pedestals, the DH5908S wireless data acquisition device can run synchronously with the scraper and is used to collect experimental data in real time. For strain measurement, a sampling frequency of 1000 Hz is taken. In addition, the experimental system is equipped with wireless transmitter and wireless receiver intended for remote data transmission. The strain data are stored in the on-site PC.

As for normal working state of the scraper conveyor, the strain signals of sensor points 1 and 2 are obtained. Figure 7 shows a comparison of experimental results with simulation results of the dynamic model. For different measurement points, the experimental strain values show consistent change patterns with the simulation results. Considering the experimental data and simulation results
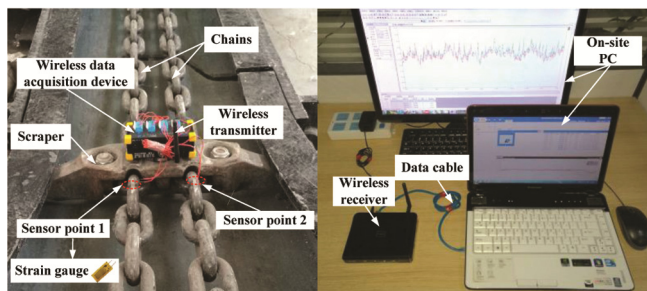
separately, good agreement between tension variation of sensor points 1 and 2 is obtained. Hence, the following conclusions can be made: (1) the established multibody dynamic model of RCTS can efficiently simulate the actual production environment and (2) the left single-chain subsystem and the right single-chain subsystem of RCTS are similar in dynamic behaviours.

An abnormal tension variation of RCTS usually appears if chain faults occur during coal transportation, and can be directly reflected by the strain signals of the scraper chain. With respect to the above-mentioned experimental set-up, the chain fault positions are shown in Figure 8. Here we analyse two typical fault conditions during the whole experiment, namely chain breakage and chain jam with a running period of the actual test process of 3 s. To evaluate the tension features of the scraper chain, strain data analyses for two sensor points are performed.

As depicted in Figure 8, the RCTS operates in normal operation, and the strain values of sensor points 1 and 2 show normal fluctuation within the range 0–2 s. Subsequently, the strain values show sudden changes when chain faults occur at the time point of 2 s, and the fault time interval is 2–3 s. As shown in Figure 8 *a*, when chain breakage occurs at the right single-chain subsystem, the strain measurement curve for tension variation of sensor point 2 shows an obvious downward trend in the fault time interval. Accordingly, affected by the right single-chain subsystem, the scraper chain at sensor point 1 of the left single-chain subsystem is jammed, and the strain value of sensor point 1 shows an obvious upward trend. Moreover, when a chain jam occurs, both of the single-chain subsystems are jammed, and tension variation of sensor points 1 and 2 shows an obvious upward trend (Figure 8 *b*).

To summarize, compared with the normal working state, the evaluation criteria of failure type for chains at fault positions are: (1) occurrence of chain breakage will cause a marked downward trend of tension in the fault time interval, and (2) chain jam will cause a marked upward trend of tension in the fault time interval. Hence, the above experimental study provides the necessary basis for verifying the effectiveness of our proposed fault detection scheme.

*Tension estimation*

After a normal starting-up period, the RCTS runs smoothly at constant speed. We divide the whole time interval (0, 4.1 s) into $N$ time points ($t_i = t_0 + i \cdot h$), where $h = 0.01$ s, $N = 410$, $t_0 = 0$. In this study, the time interval we concern is (1, 4.1 s), when the sprocket rotates at a constant speed. The TDEA proposed is first applied for tension monitoring of the scraper chain by estimating the unknown longitudinal contact forces of the contact points through $q$ available states. To better highlight the
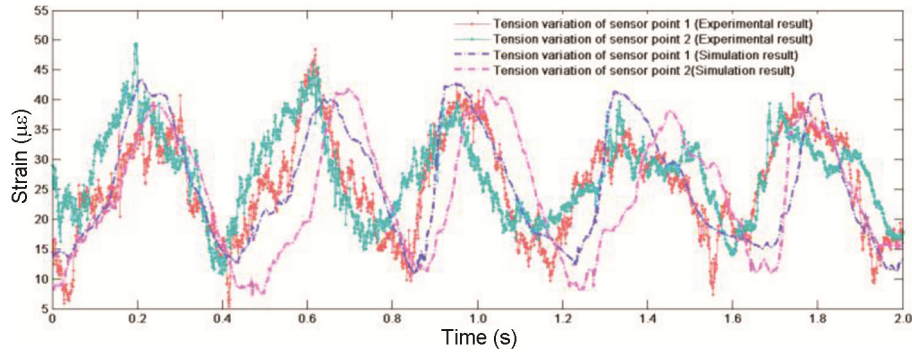


**Figure 6.** Experimental set-up of strain measurement.

**Figure 7.** Tension variation of sensor points under normal working condition.
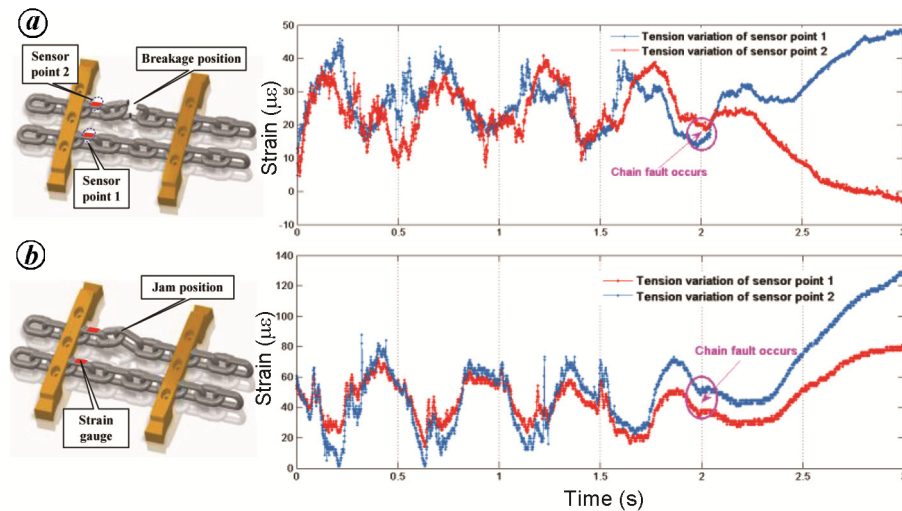


**Figure 8.** Tension variation of sensor points for (*a*) chain breakage and (*b*) chain jam.

superiority of the TDEA, the auto-regressive and moving average (ARMA) model[22] is applied to predict the tension of different contact points. Using eq. (9), we can predict tension variation of the RCTS at time interval (1, 4.1 s) based on the tension values of the *n* (146) contact points at time interval (1, 2 s); the tension values at time interval (1, 2 s) can be obtained from simulation outputs of the multibody dynamics model.

$$X_t = \phi_1 X_{t-1} + \cdots + \phi_\partial X_{t-\partial} + \varepsilon_t - \theta_1 \varepsilon_{t-1}$$

$$-\theta_2 \varepsilon_{t-2} - \cdots - \theta_\beta \varepsilon_{t-\beta}, \tag{9}$$

where $X_t$ denotes a time series, $\phi_i$ and $\theta_i$ denote the undetermined coefficients, $\varepsilon_t$ is the independent error term.

The upper chain subsystem of the left single-chain subsystem is more susceptible to external factors, and we choose contact points of the upper chain subsystem as the research object, that is, contact point $i(1 \leq i \leq 73)$. The longitudinal tension distribution rules are discussed when $t = 3$ s, which is used as the research sample time point to validate the estimated effectiveness of the tension distribution estimation method. Figure 9 presents the estimated

contact forces of each contact point at different values of $I_0$ based on TDEA, and estimated tension of the RCTS is defined as $\bar{F} = [\bar{F}_1; \bar{F}_2; \cdots \bar{F}_{\omega-1}; \bar{F}_\omega]$ ($\omega = n/2$). The estimated tension reveals a consistent and nonlinear trend for different values of $I_0$: as the contact points of the upper chain subsystem are considered in ascending order, the estimation result reveals an overall increase. Obviously, the tension distribution rules depend on where the contact points are located, and the minimum and maximum values occur at spatial contact points 1 and 73 respectively. Contrasting the estimated results of different contact points $i$, it indicates that all the contact pairs of the RCTS move towards the higher-tension positions counterclockwise during the practical operation process. Moreover, the actual tension $f$ is defined as $f = [f_1; f_2; \cdots f_{\omega-1}; f_\omega]$ and is obtained through the virtual prototype model. The predicted tension $F$ is defined as $F = [F_1; F_2; \cdots F_{\omega-1}; F_\omega]$ and is predicted using the ARMA model.

To validate the consistency of estimation performance, comparisons among $f$, $F$ and $\bar{F}$ are made, corresponding to the simulated trajectories displayed in Figure 9. For quantitative evaluation of the estimation precision at different values of $I_0$, the root mean squared (RMS) errors
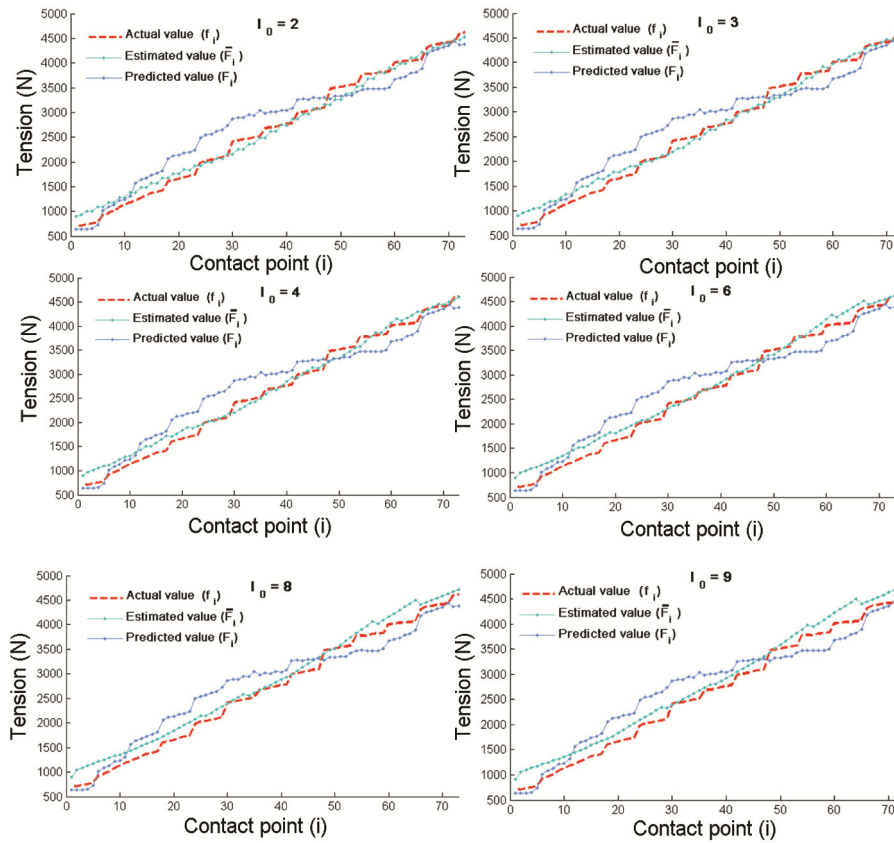
**Figure 9.** Tension variation trajectories.

| $I_0$ | $q$ | $\zeta_F$ | $\delta_F$ |
|---|---|---|---|
| 2 | 15 | 0.0487 | |
| 3 | 10 | 0.0503 | |
| 4 | 7 | 0.0513 | 0.1119 |
| 6 | 5 | 0.0561 | |
| 8 | 4 | 0.0681 | |
| 9 | 3 | 0.0747 | |

$\zeta_F$ and $\delta_F$ are calculated between $\bar{F}$ and $f$, as well as $F$ and $f$ respectively, as follows

$$\text{RMS } \zeta_F = \sqrt{\frac{1}{\omega}\sum_{i=1}^{\omega}(\bar{F}_i - f_i)^2} \Big/ \sqrt{\frac{1}{\omega}\sum_{i=1}^{\omega}f_i^2}, \qquad (10)$$

$$\text{RMS } \delta_F = \sqrt{\frac{1}{\omega}\sum_{i=1}^{\omega}(F_i - f_i)^2} \Big/ \sqrt{\frac{1}{\omega}\sum_{i=1}^{\omega}f_i^2}. \qquad (11)$$

Table 1 presents the parameters set to evaluate the estimation errors of tension. Clearly, the RMS errors $\zeta_F$ show low values, revealing the reliable estimation ability to monitor tension variation and obtain unknown contact forces of all contact points for the upper chain subsystem. In particular, for time point $t = 3$ s of the simulation

process, the values of $\zeta_F$ are prone to higher levels as $I_0$ increases from 2 to 9, i.e. the estimation errors become larger with the increase in $I_0$. However, TDEA still shows excellent performance in force estimation of the upper chain subsystem when $I_0 = 9$, for which the value of $\zeta_F$ is 0.0747. Correspondingly, the approximate value of $\delta_F$ is 0.1119, based on which superiority of the proposed TDEA can be confirmed. Moreover, the proposed TDEA is capable of reducing the number of tension sensors used in actual engineering applications.

## Detection process

The system performance of the mathematical model relies heavily on the stiffness coefficient of each discrete element. In this sense, matrix $K$ can be utilized to determine the working state of each element and judge whether chain faults occur. Based on the mathematical model, chain faults appearing in RCTS can be easily determined by setting different values of stiffness coefficients $k_i$. In Figure 9, for the upper chain subsystem of different $I_0$, contact point $n/2$ bears the maximum tension and serves as the most vulnerable position of the chain faults. The objective of this study is to detect the occurrence of chain failure in real time by tension monitoring of contact point $n/2$ based on the proposed TDEA. We determined
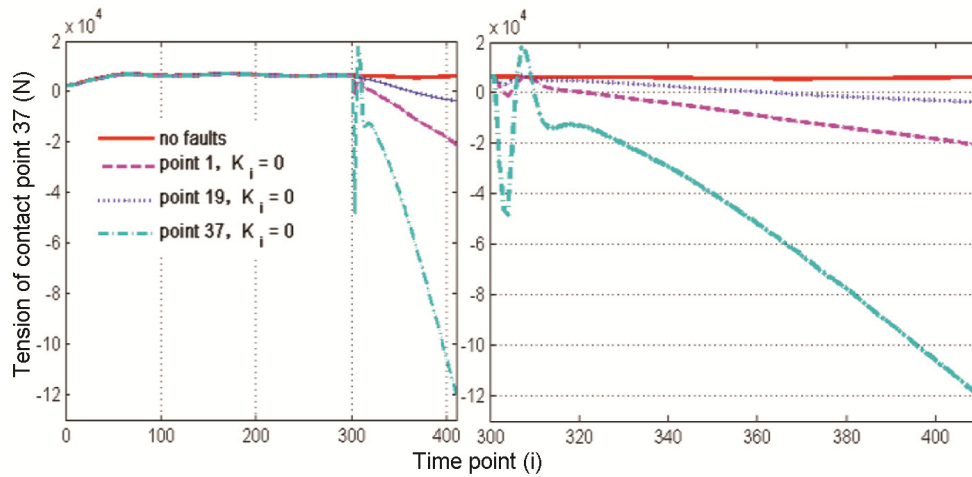
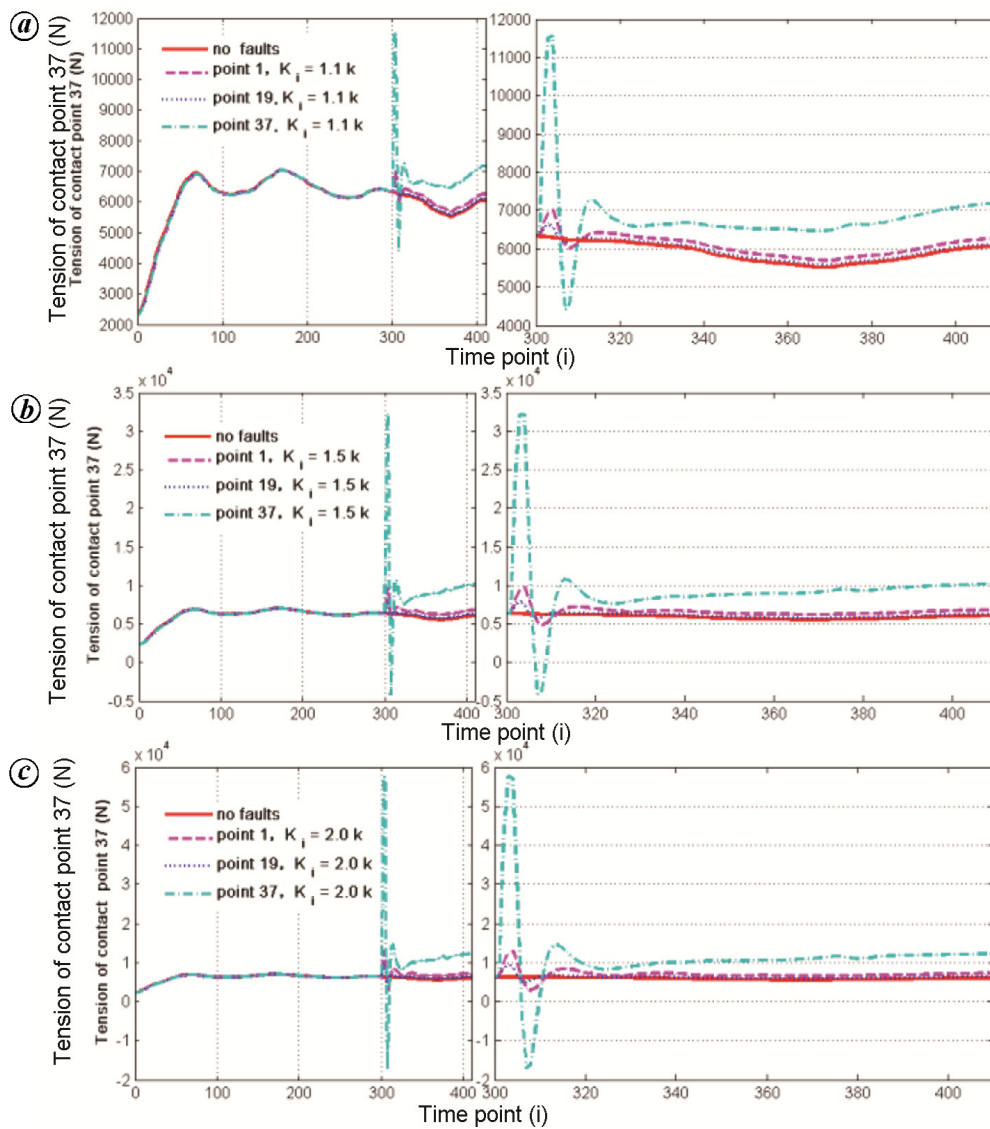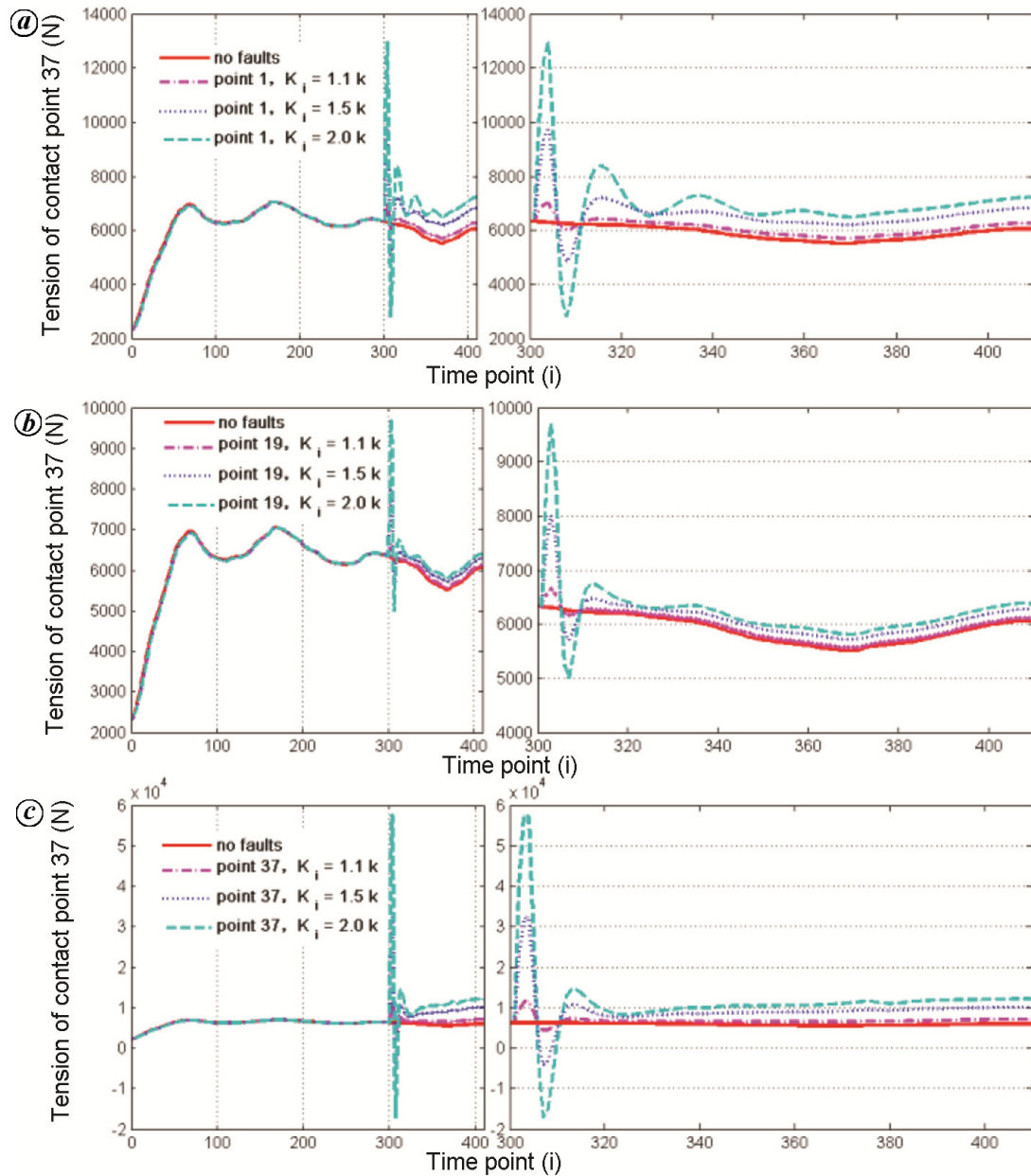**Figure 10.** Tension variation for chain breakage.



**Figure 11.** Tension variation of chain jam for (*a*) $k_i = 1.1k$, (*b*) $k_i = 1.5k$ and (*c*) $k_i = 2.0k$.

**Figure 12.** Tension variation of chain jam for different fault positions: (**a**) point 1, (**b**) point 19 and (**c**) point 37.

that the whole operating time interval (0, 4.1 s) is divided into 410 time points and that no chain faults occur from time point 1 to 300 (0 to 3.0 s). Subsequently, chain faults are triggered at time point 301, and the whole process lasts 1.1 s (time points 301–410). For different values of $I_0$, we assume that chain breakage or chain jam occurs at three representative contact points, namely contact points 1, $(n + 2)/4$ and $n/2$, which are located at the head, middle and tail of the upper chain subsystem respectively. Referring to Table 1, to ensure accuracy of the fault detection process, we take the value of $I_0$ as 2, where RM Serror $\zeta_F$ can reach up to 0.0487. Thus, we choose contact points 1, 19 and 37 as the fault positions

to trigger chain faults by setting parameter $k_i$ of the discrete element for each point.

When chain breakage occurs, two contacting chains will be separated. Herein, we set $k_i = 0$ at time point 301. Given the tension trajectory on the premise of no chain faults ($k_i = k$), Figure 10 shows the estimated tension variation of contact point 37 for different fault positions. As shown, the RCTS is in normal operation within the range 0–3 s. To analyse the detection results of chain breakage in more detail, we consider 1.1 s (time points 300–410) for analysis. Once chain breakage occurs at contact point 1, 19, or 37, the tension of contact point 37 exhibits a consistent sudden change at 3.01 s (trigger time point).

Subsequently, the tension signals exhibit instantaneous unstable fluctuations from 3.01 to 3.2 s. To verify the effectiveness of the proposed TDEA for fault detection, our study focuses on the stable phase of fault occurrence within the range 3.2–4.1 s. In the stable stage of chain breakage, fault positions affect the tension of contact point 37 in different degrees. The tail position (contact point 37) has the greatest impact on tension of contact point 37, whereas the middle position (contact point 19) has the least impact. The tension of contact point 37 shows consistent marked downward trend when chain breakage occurs at different fault positions, which is in agreement with the evaluation criteria (1) corresponding to Figure 8.

When chain jam occurs at different fault positions, the trajectories in Figure 11 *a–c* separately depict of the estimated tension variation of contact point 37 by setting $k_i = 1.1k$, $1.5k$ and $2k$ at time point 301. Similar to chain breakage, to obtain a more detailed description of the detection results, we consider the stable stage of chain breakage for analysis. Within the range 3.2–4.1 s, for different levels of $k_i$, the fault positions affect the tension of contact point 37 to different degrees. Taking $k_i = 1.1k$ as the reference, the head position (contact point 1) causes less impact on tension variation of contact point 37 than the tail position (contact point 37), and a greater impact than the middle position (contact point 19). Based on the tension trajectory when no chain faults occur ($k_i = k$), the tension of contact point 37 shows consistent marked upward trend when chain jam occurs at different fault positions, in agreement with the evaluation criteria (2) of Figure 8. For $k_i = 1.5k$ and $2.0k$, the above rules are also applicable. To study the effect of parameter setting on the detection effect, a more detailed description for chain jam is shown in Figure 12 *a–c*. For the same jammed position, i.e. contact point 1, 19 or 37, it can always be found that a larger $k_i$ will bring a more obvious tension variation of contact point 37.

Based on the above analysis, when chain breakage or chain jam occurs, the estimated tension variation of contact point 37 is consistent with the evaluation criteria of chain faults. In particular, the detection performance is not affected by fault positions and stiffness parameter $k_i$. Hence, the proposed observer-based TDEA is effective at identifying the occurrence of chain faults and detecting the type of chain faults of the RCTS.

## Conclusion

During the actual operation of the RCTS, the dynamic performance of the scraper chain is difficult to obtain. To address this, a virtual prototyping model is presented here using ADAMS software by fitting the actual behaviour of the RCTS. The efficiency of the virtual prototyping model is verified by comparison with experimental results.

The chain system was discretized into multiple elements to build the mathematical model. A mathematical model-based observer has been designed to evaluate the tension distribution rules of the RCTS, based on which we propose an observer-based TDEA. Moreover, the simulation results show that accurate tension distribution estimation is achieved, thereby providing a reference for tension monitoring and fault detection of the RCTS.

Thus, fault detection of the scarper chain can alert us to the occurrence of chain breakage and chain jam acting on fault locations in real time and can efficiently distinguish the two typical chain faults. Currently, it is difficult to verify the reliability of the proposed fault detection scheme using field experiments. Hence, fault detection of the scraper chain based on experimental data will be considered in the near future.

*Conflicts of interest:* The authors declare no conflict of interest.

1. Wösle, M. and Pfeiffer, F., Dynamics of multibody systems containing dependent unilateral constraints with friction. *J. Vib. Control*, 1996, **2**, 161–192.
2. Pfeiffer, F. and Glocker, C., *Multibody Dynamics with Unilateral Contacts*, John Wiley, 1996, p. 262.
3. Zhu, L. *et al.*, Combined finite element and multi-body dynamics analysis of effects of hydraulic cylinder movement on ploughshare of horizontally reversible plough. *Soil Tillage Res.*, 2016, **163**, 168–175.
4. Wauge, D. H., Modelling of an armoured face conveyor. Department of Mechanical Engineering, The University of Queensland, 2003.
5. Nie, R. *et al.*, Modelling of the transmission system in conveying equipment based on Euler method with application. *Proc. Inst. Mech. Eng. Part K J. Multi-body Dyn.*, 2014, **228**, 294–306.
6. He, B. *et al.*, Dynamic behaviour modelling and simulation of the chain transmission system for an armoured face conveyor. In Proceeding of the 2009 IEEE 10th International Conference on Computer-Aided Industrial Design and Conceptual Design, Wenzhou, People's Republic of China, 2009, pp. 1000–1004.
7. Jiang, S. B. *et al.*, Multi-body dynamics and vibration analysis of chain assembly in armoured face conveyor. *Int. J. Simul. Model.*, 2017, **16**, 458–470.
8. Myszkowski, M. and Loehning, D., Chain force measurements on armoured face conveyors and coal plows in heavy-duty longwalls. *CIM Bull.*, 2001, **94**, 72–75.
9. Wang, H., Zhang, Q. and Xie, F., Dynamic tension test and intelligent coordinated control system of a heavy scraper conveyor. *IET Sci. Meas. Technol.*, 2017, **11**, 871–877.
10. Krebs, S. *et al.*, Reduced-order hybrid interval observer for verified state estimation of an induction machine. *Control Eng. Pract.*, 2016, **57**, 157–168.
11. Rajshekhar, G. and Rastogi, P., Phase estimation using a state-space approach based method. *Opt. Lasers Eng.*, 2013, **51**, 1004–1007.
12. Mata-Machuca, J. L., Martínez-Guerra, R. and Aguilar-Sierra, H., Fault estimation using a polynomial observer: a real-time application. *IFAC Proc. Vol.*, 2012, **45**, 552–557.
13. Sun, S., Ma, X. M. and Yang, Z. S., Diagnosis of coal scraper conveyor based on fuzzy fault tree. In Seventh International Conference on Measuring Technology and Mechatronics Automation, Nanchang, People's Republic of China, 2015, pp. 392–395.

14. Zhang, Y. *et al.*, Fuzzy neural network fault diagnosis and online vibration monitoring system for the coal scraper conveyor based on rough set theory. In Proceedings of the 32nd Chinese Control Conference, Xi'an, People's Republic of China, 2013, pp. 6134–6138.

15. Gong, X., Ma, X., Zhang, Y. and Yang, J., Application of fuzzy neural network in fault diagnosis for scraper conveyor vibration. In International Conference on Information and Automation, Yinchuan, People's Republic of China, 2013, pp. 1135–1140.

16. Xue, S., Li, X. and Xu, X., Fault tree and bayesian network based scraper conveyer fault diagnosis. In Proceedings of the 22nd International Conference on Industrial Engineering and Engineering Management 2015, Singapore, 2016, pp. 783–795.

17. Sedighi, T., Foote, P. D. and Sydor, P., Feed-forward observer-based intermittent fault detection. *CIRP J. Manuf. Sci. Technol.*, 2017, **17**, 10–17.

18. Emami, K., Fernando, T., Nener, B., Trinh, H. and Zhang, Y., A functional observer based fault detection technique for dynamical systems. *J. Franklin Inst.*, 2015, **352**, 2113–2128.

19. Hippmann, G., An algorithm for compliant contact between complexly shaped surfaces in multibody dynamics. *Multibody Dyn.*, 2003, **12**, 345–362.

20. Beyhan, S., Runge-Kutta model-based nonlinear observer for synchronization and control of chaotic systems. *ISA Trans.*, 2013, **52**, 501–509.

21. Zhang, X. *et al.*, Tension monitoring for the ring chain transmission system using an observer-based tension distribution estimation method. *Adv. Mech. Eng.*, 2017, **9**, 1687814017727251.

22. Xu, S. and Zeng, B., Network traffic prediction model based on auto-regressive moving average. *J. Networks*, 2014, **9**, 653–659.